

Thermal properties of porous sodium polyacrylate/silica nanocomposites^{*)}

Alina V. Korobeinyk^{1, **)} (ORCID ID: 0000-0002-7248-0627), Gabriella Yurchenko¹⁾ (0000-0003-0866-8219), Alexander Matkovsky¹⁾ (0000-0001-7847-1468), Valentin Tertykh¹⁾ (0000-0003-3253-0279)

DOI: <https://doi.org/10.14314/polimery.2023.2.5>

Abstract: Porous sodium polyacrylate/silica (SPA/SiO₂) nanocomposites were obtained in a single-stage sol-gel process involving the acidic hydrolysis of tetramethoxysilane (TMOS) in the presence of SPA. The TMOS/SPA molar ratio ranged from 2:1 to 8:1. The physical and thermal properties of the nanocomposites were characterized by FTIR, SEM, TGA and adsorption analysis (BET, BJH). The mechanical and chemical treatment of the composite after the synthesis increased its specific surface area without significantly changing thermal properties. The process enables pore size control.

Keywords: sol-gel process, porous nanocomposites, sodium polyacrylate.

Właściwości termiczne porowatych nanokompozytów poliakrylan sodu/krzemionka

Streszczenie: Porowate nanokompozyty poliakrylan sodu/krzemionka (SPA/SiO₂) otrzymano w jedno-etapowym procesie zol-żel polegającym na kwaśnej hydrolizie tetrametoksylanu (TMOS) w obecności SPA. Stosunek molowy TMOS/SPA wynosił od 2:1 do 8:1. Właściwości fizyczne i termiczne otrzymanych nanokompozytów scharakteryzowano za pomocą FTIR, SEM, TGA i analizy adsorpcyjnej (BET, BJH). Mechaniczna i chemiczna obróbka kompozytu po procesie syntezy zwiększyła jego powierzchnię właściwą bez znaczącej zmiany właściwości termicznych. Proces umożliwia kontrolę wielkości porów.

Słowa kluczowe: proces zol-żel, porowate nanokompozyty, poliakrylan sodu.

Polymeric polyelectrolytes are attractive materials for a wide range of application such as catalysis, sorbents, and separation processes. Improving the thermal and mechanical properties of polymeric polyelectrolytes by embedding in inorganic matrices is one of the possible ways to expand their applications. Sol-gel methods [1] facilitate the formation of composite materials with excellent compatibility between organic and inorganic components in the final silica based composite [1]. Therefore greater attention has been paid to the study of silica based organic-inorganic nanocomposites with unique mechanical, photoelectric and thermal properties, prepared via sol-gel process [2, 3].

Poly(acrylic acid) (PAA) is an important water-soluble polyelectrolyte polymer widely used as an adhesive and super-adsorbent polymer due to the presence of pendant carboxyl groups. The sodium salt of PAA, sodium polyacrylate (SPA), exhibits great promise as an ion-exchange material [4, 5]. SPA can be added directly to typical sol-gel

formulations, due to its solubility in water, and various organic-inorganic compositions can be easily prepared [1, 6].

In this paper sol-gel process was used to obtain porous sodium polyacrylate/silica (SPA/SiO₂) nanocomposites. The materials were examined by TGA, TEM, IR, and low temperature nitrogen adsorption. Also, the kinetic parameters of thermal degradation have been analyzed.

EXPERIMENTAL PART

Materials

Sodium polyacrylate (SPA) and tetramethoxysilane (TMOS) were supplied by Sigma-Aldrich (Germany). Ethanol (EtOH) was delivered by Macrochim Reagents Company (Kyiv, Ukraine). 0.1 N solutions of nitric (HNO₃) and hydrochloric (HCl) acids were purchased from Reachim Reagents Company (Kyiv, Ukraine).

¹⁾ O.O. Chuiko Institute of Surface Chemistry of National Academy of Science of Ukraine, 17, Gen. Naumov Str., 03164 Kyiv, Ukraine.

^{*)} The material contained in the article was presented at the 64th Scientific Congress of the Polish Chemical Society (PTChem), September 11–16, 2022, Lublin, Poland.

^{**)} Author for correspondence: alina.v.korobeinyk@gmail.com

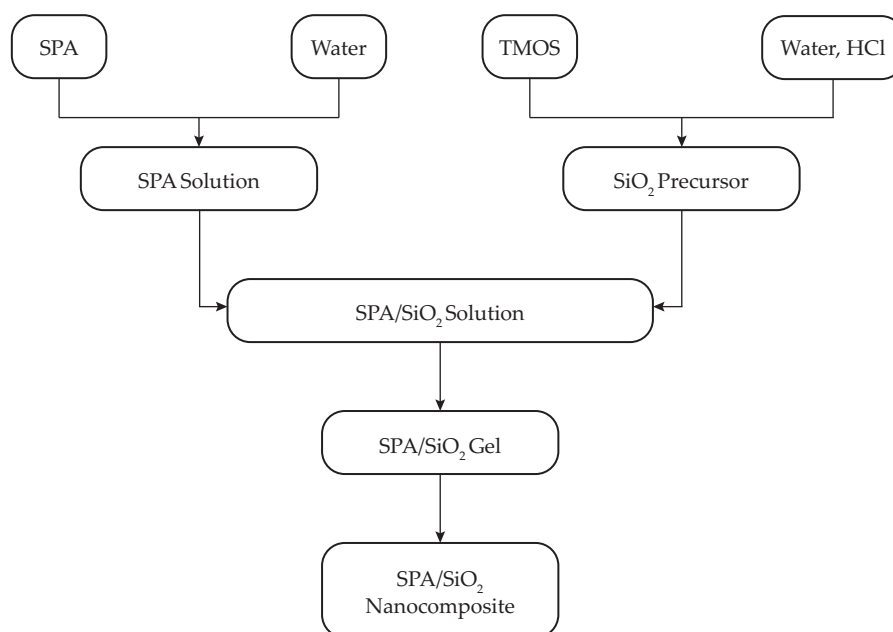


Fig. 1. Scheme for obtaining SPA/SiO₂ nanocomposites Na rys. w pierwszej ramce z lewej strony zamiast SP powinno być SPA

Nanocomposites preparation

The porous sodium polyacrylate/silica nanocomposites (SPA/SiO₂) were obtained by the sol-gel method [1]. The TMOS solution was hydrolyzed with a mixture of deionized water and 0.1 NHCl and stirred in glass beaker at room temperature for 2 min until the clear solution was obtained. Appropriate amount of SPA in deionized water was added to the silica precursor and the mixture was stirred at ambient temperature for 30 s then held until a homogeneous and transparent gel was obtained. The gel was then treated in two different ways: i) the gel was left to age at room temperature for 7 days, after aging the samples were milled and dried at 105°C under vacuum for 9 h; ii) the gel was mixed, soaked in a 50/50 mixture (% v/v) of EtOH and (0.1 N) HNO₃ for 1 min, and then rinsed with deionized water through a glass filter ($d_{\text{pore}} = 40 \mu\text{m}$) [6], after 7 days, all samples were ground and dried at 105°C under vacuum for 9 h. For comparison, a sample without the polymeric compound was prepared. Fig. 1 shows the scheme for obtaining SPA/SiO₂ nanocomposites, and Table 1 summarizes the proportions of reagents.

Methods

FT-IR analysis of SPA/SiO₂ nanocomposites was performed by using the KBr pellet method (Thermo Nicolet NEXUS Spectrophotometer, USA). The surface structure and morphology of the SPA/SiO₂ nanocomposites were analyzed using a Tesla BS30 scanning electron microscope (SEM) (Tesla, USA) with "Satellite"-1 digital system. Thermogravimetric analyses (TGA) were carried out with a Q-1500D thermogravimetric analyzer (MOM, Hungary) at a heating rate of 10°C/min and the temperature range from 20 to 1000°C in nitrogen flow. Several mathematic models from Freeman-Carroll [7], Friedman [8], and Chang [9] have been used for calculation the nanocomposites pyrolysis kinetic. Nitrogen adsorption-desorption isotherms were measured at -196°C using a Kelvin 1042 analyzer (COSTECH, Italy) where the samples were degassed at 120°C for 2 h prior to measurement. The specific surface area was obtained from the adsorption isotherm by the Brunauer-Emmett-Taylor (BET) method [10]. The pore size distribution was calculated using the desorption isotherm according to the Barrett-Joyner-Halenda (BJH) method [11].

Table 1. The formulation of SPA/SiO₂ nanocomposites

Sample	SPA mol	TMOS mol	Water mol	HCl millimole	Gel process
SPAS - 0	0	0.1	1.55	0.9	-
SPAS - 1	0.0125	0.1	1.66	0.9	-
SPAS - 2	0.025	0.1	1.78	0.9	-
SPAS - 3	0.05	0.1	2.02	0.9	-
SPAS - 4	0.0125	0.1	1.66	0.9	+
SPAS - 5	0.025	0.1	1.78	0.9	+
SPAS - 6	0.05	0.1	2.02	0.9	+

RESULTS AND DISCUSSION

Structure analysis

Fig. 2 shows SEM images of two types of porous SPA/silica nanocomposites with different silica content with or without a gel processing step. Significant differences in the particles shape and size and the nanocomposite structure can be observed with a change in the silica content. As the silica content decreases, the particles transform from small spheres that are packed into an amorphous structure to irregular, sharp glassy flakes. There is no dramatic effect of the gel processing step on the structure and shape of the particles, but a slight increase in particle size can be observed. Primary silica structures are formed already at the gelation stage in sol-gel synthesis, and treatment with a mixture of ethanol/nitric acid accelerates gel curing [12], removes unbound polymer and protonates hanging acrylic groups in (poly)acrylic. The increase in particle size in composites because of wet gel treatment was confirmed by SEM and may indicate acceleration of the condensation process as part of the sol-gel transition.

The lack of a strong effect of gel treatment on the structure of the obtained composites was also confirmed by the comparison of nitrogen adsorption-desorption isotherms in Fig. 3. As can be seen in Fig. 3, isotherms are of different types according to the IUPAC classification [10]; the isotherm for SPAS-1 and SPAS-4 is type I, SPAS-2 and SPAS-5 is type II, and for SPAS-3 and SPAS-6 is type IV. Hysteresis loops occur in all isotherms at high relative pressures (0.5–0.9 p/p_0). The calculated values of adsorption, specific surface area and pore diameters (Table 2) indicate that the samples are mesoporous [10]. With respect to the nitrogen adsorption isotherm (not shown here), the SPAS-0 sample is a non-porous material ($S_{sp} = 212 \text{ m}^2/\text{g}$).

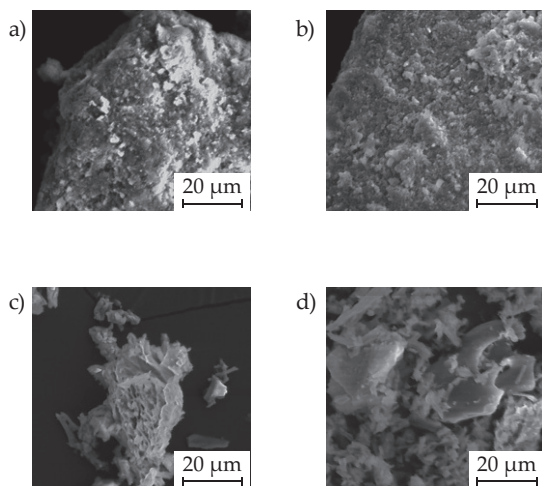


Fig. 2. SEM images of porous SPA/silica nanocomposites: a) SPAS-2, b) SPAS-5, c) SPAS-3, d) SPAS-6

Specific surface area

Values of the specific surface area in untreated samples rises with the increase in polymer content from $285 \text{ m}^2/\text{g}$ for SPAS-1 up to $315 \text{ m}^2/\text{g}$ for SPAS-2 then the SPAS-3 this value fall to $84 \text{ m}^2/\text{g}$ (Fig. 4a) which may confirm that polymer aggregates with the interparticle space between the particles of silica and can act as a template during sample curing. This can be supported by comparison of the specific surface values for an initial (Fig. 4a) and wet gel treated samples (Fig. 4b). In treated samples the SPAS-4 shows highest values in specific surface and relatively small pore volume vs. pore diameter (Table 2). With an increase in polymer concentration in the initial samples undergoing gel processing shows a decrease in the specific surface area and increase in pore volume and diameter (Table 2). Therefore, lower doping levels of the polymer in sol-gel mixture leads to formation of smaller silica particles with smaller pore channels, which are possibly formed around the polymer, whereas the higher polymer concentration promotes formation of a porous system with bigger pore diameter and higher adsorptive capacity.

In calculation of the fractal dimensions, which is the characteristic of the sample surface relief, equation (1) is used when the dispersion interactions between the solid and film of the liquid nitrogen adsorbed dominates, while equation (2) corresponds to an adsorption state in which the capillary forces are dominant [12, 13]

$$a/a_m \approx [\ln(P_s/P)]^{-(3-D)/3} \quad (1)$$

$$a/a_m \approx [\ln(P_s/P)]^{-(3-D)} \quad (2)$$

where D – the value of fractal dimension; a – the value of adsorption at relative pressure P/P_s (P – the value of the equilibrium pressure and P_s – the pressure of the saturated nitrogen vapors at temperature of the measurement) and a_m – the monolayer capacity determined from BET. The shape of the nitrogen adsorption isotherms confirms the capillary condensation phenomena is operating in the samples therefore equation 2 was used for the calculation of fractal dimensions of the samples. The D -values for the studied samples are in the range of 2.44–2.82 (Table 2), and the most ulcerated surface of the samples is that with the lowest polymer loading. It is significant that the fractal dimension is dependent on the ratio of the reacting components and independent from the gel processing step, which may confirm the assumption about immutability of the sample's structural properties during gel processing procedure.

The type of nitrogen adsorption-desorption isotherms depends on the silica/polymer ratio, but the gel treatment step led to a higher adsorption value in all cases (Fig. 3b). It is assumed that such an increase in the adsorption value occurs because of the removal of unbound polymer from the composite surface during gel treatment, which can be confirmed by SEM image analysis, where

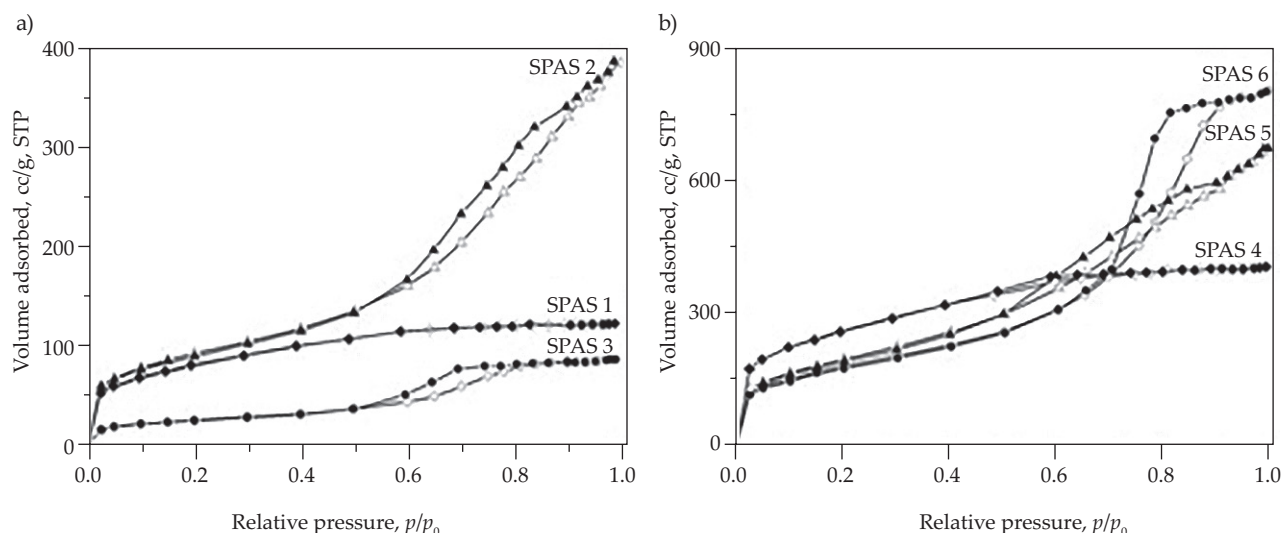


Fig. 3. Nitrogen adsorption-desorption isotherms: a) SPAS-1, SPAS-2, SPAS-3; b) SPAS-4, SPAS-5, SPAS-6

silica structures predominate in the agglomerates of the treated composites, showing as an increase in the silica flakes number.

FT-IR analysis

SPA/SiO₂ nanocomposites were characterized by FT-IR spectroscopy as shown in Fig. 5. The spectra show strong reflection bands in the region below 1100 cm⁻¹ corresponding to vibrations of the framework-forming SiO₄ tetrahedra, and the bands in the 1600–1700 and 3200–4000 cm⁻¹ regions originate from bending and stretching vibrations in Si–OH groups and physisorbed water in the composites [15]. The peak at 1560 cm⁻¹ is typical of asymmetric stretching vibration of carboxylic (ν_a COO⁻) groups in the polyacrylic polymer. The bands at 2920 cm⁻¹ and in the range 1400–1500 cm⁻¹ are characteristic of stretching and deformation vibrations of C–H bonds [16]. Also, a peak at 1365–1325 cm⁻¹ relates to vibration of δ (CH) group. SPA was successfully introduced in porous organic-inorganic composites during the sol-gel process.

Thermogravimetric analysis

Thermal decomposition of untreated SPA/SiO₂ nanocomposites (Fig. 6a) can be divided into three stages (70–200, 280–380 and 420–530°C). The exception is the SPAS-3 sample, which thermal decomposition takes place in four stages, probably due to the higher polymer content. The first stage of weight loss at 70–200°C is due to the desorption of water. The next two stages in the high temperature region correspond to the thermal decomposition of the SPA segments [15]. Comparing the thermal decomposition of silica-polymer composites and poly(acrylic acid), it was found that the formation and decomposition of anhydride in poly(acrylic acid) (at 170 and 230°C, respectively) [16] moves towards a higher temperature (280–380°C) for the composite. Such an improvement in the thermal stability of polymers embedded in

a silica matrix has previously been described as the “trapping effect” of SiO₂ [17].

TG curves for treated SPA/SiO₂ composites (Fig. 6b) shows two stages of weight loss at 40–200 and 270–390°C, respectively. Nonoccurrence of the third stage of thermal decomposition in treated samples can be attributed to minor amounts of free polymer not embedded in the silica matrix, which is due to the solvent processing of the wet gel.

Data from the TG curves (Fig. 7) were differentiated to determine the actual number of thermal degradation process steps. The percentage weight loss varied depending on the temperature, and the individual stages of thermal decomposition are given in Table 3. Increasing the specific surface area of the nanocomposites shifts the water desorption stage to lower temperature, which is easily seen in Tables 2 and 3.

In thermal analysis, apart from mass changes, valuable information about the degradation process itself can be obtained [18]. Although the theoretical approach to thermal analysis is relatively simple and based on idealized reaction types, imperfections appear when decomposition reactions are complex [19]. Such complexity of thermal decomposition mechanisms can be caused by the presence of different functional groups, the ratio of

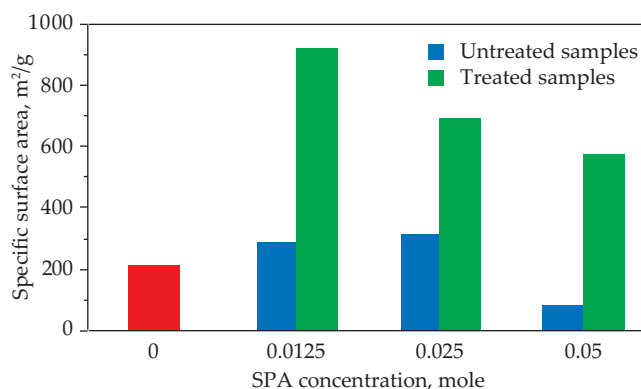
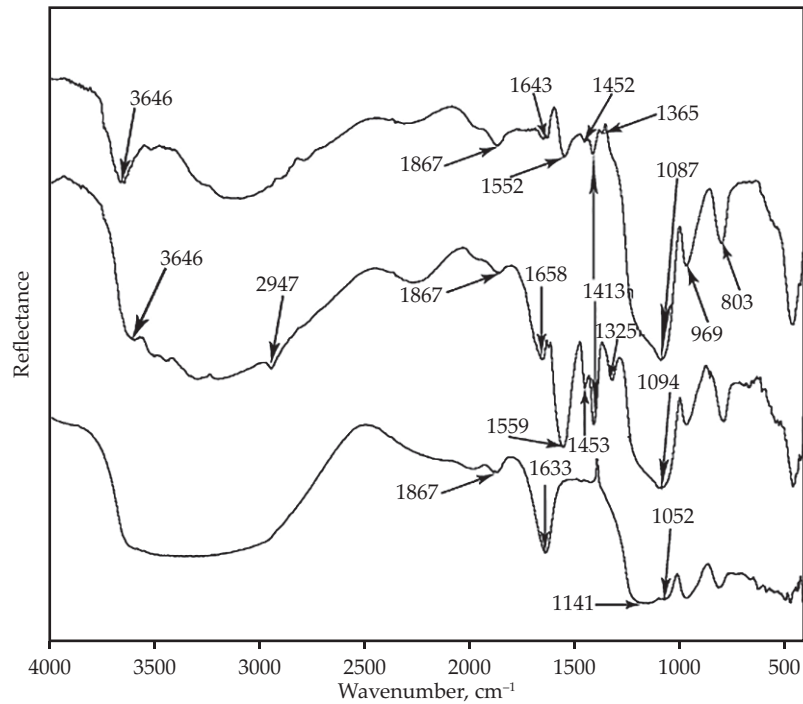
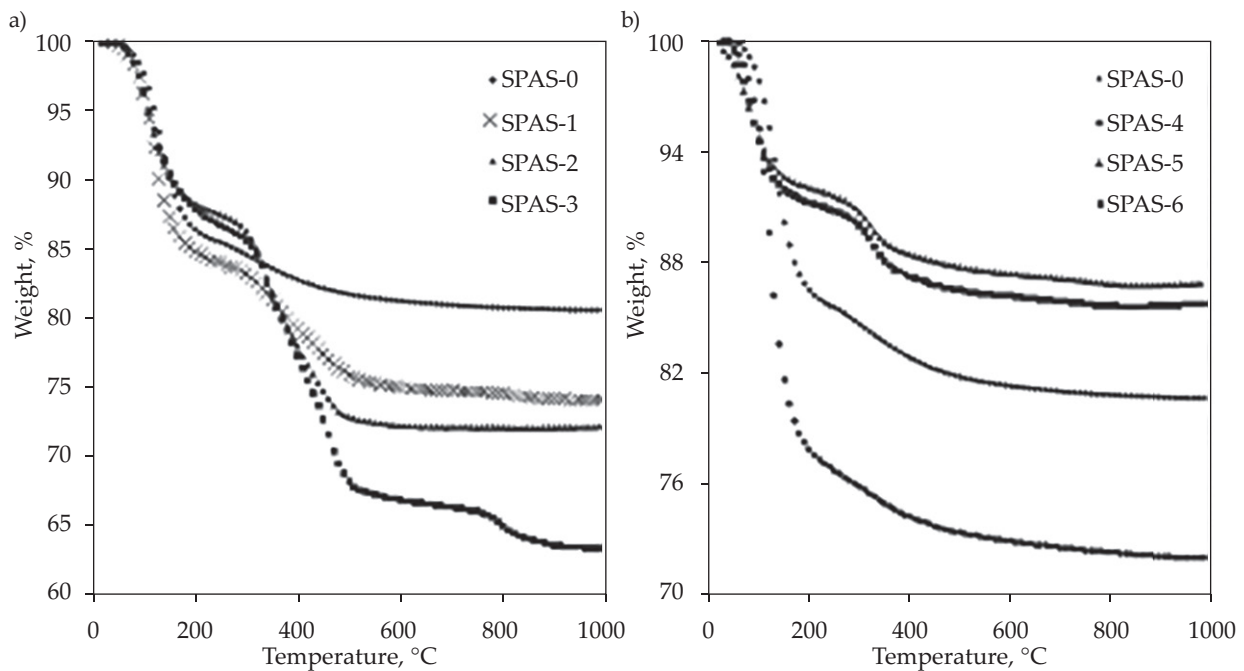


Fig. 4. The specific surface area of SPA/SiO₂ differing in SPA content

Table 2. Structural-adsorption properties of porous SPA/silica nanocomposites

Sample	S_{sp} , m ² /g	V_p , cm ³ /g	d , nm	Fractal dimension in P/P _s interval	
				P/P _s	D
SPAS - 1	285	0.14	2.6 ^{a)}	0.3-0.8	2.80
SPAS - 2	315	0.58	5.6	0.35-0.8	2.44
SPAS - 3	84	0.13	5.5	0.2-0.8	2.53
SPAS - 4	920	0.31	2.8 ^{a)}	0.3-0.8	2.82
SPAS - 5	690	0.95	4.6	0.4-0.75	2.47
SPAS - 6	597	1.21	8.4	0.15-0.5	2.59

^{a)} diameter of pore were calculated by equation: $d = 4 V_p/S$ [14].

**Fig. 5.** FT-IR spectra of SPA/SiO₂ nanocomposites: a) SPAS-0, b) SPAS-3, c) SPAS-6**Fig. 6.** Thermal decomposition of SPA/silica nanocomposites: a) SPAS-0, SPAS-1, SPAS-2, SPAS-3; b) SPAS-0, SPAS-4, SPAS-5, SPAS-6

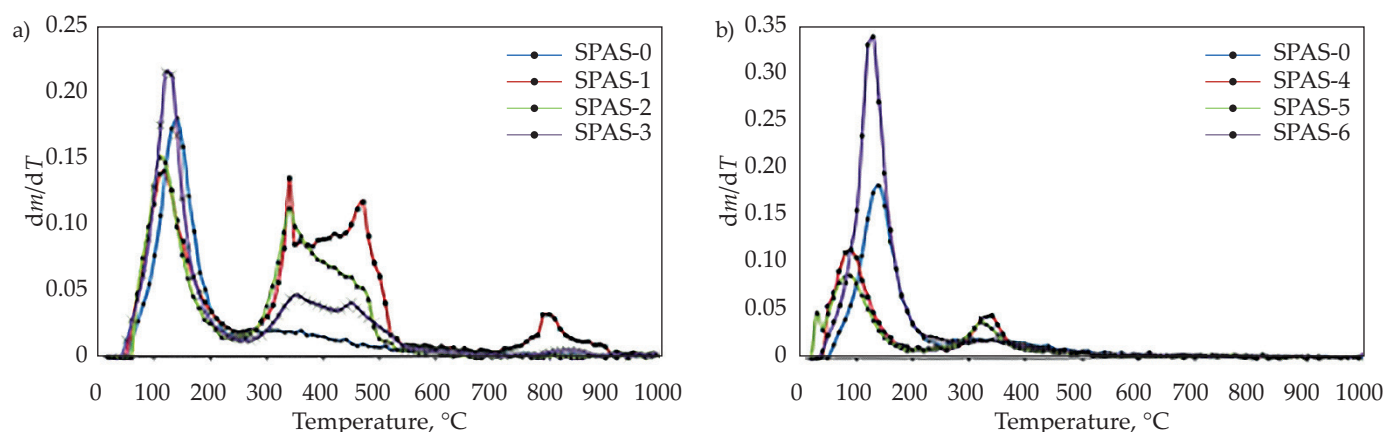


Fig. 7. DTG graphs of SPA/silica nanocomposites: a) SPAS-0, SPAS-1, SPAS-2, SPAS-3; b) SPAS-0, SPAS-4, SPAS-5, SPAS-6

Table 3. TGA data of SPA/silica nanocomposites

Sample	The first stage		The second stage		The third stage	
	Temp. range °C	Weight loss %	Temp. range °C	Weight loss %	Temp. range °C	Weight loss %
SPAS-0	70–210	13.5	–	–	–	–
SPAS-1	80–200	12.0	280–340	5.5	430–520	14.9
SPAS-2	80–190	11.3	280–380	9.2	420–510	6.8
SPAS-3	70–190	14.8	280–380	5.1	420–530	4.6
SPAS-4	40–160	8.2	280–380	4.3	–	–
SPAS-5	40–170	7.6	270–390	3.8	–	–
SPAS-6	60–200	22.0	300–390	3.6	–	–

Table 4. Characteristic temperatures and kinetic parameters of the decomposition reaction for porous SPA/silica composites under nitrogen

Samples	Temperature range, °C	Freeman-Carroll $E_a(J/mol)/n$,	Friedman $E_a(J/mol)/n$	Chang		Average E_a/n
				n^a	n^b	
SPAS-0	70–210	38 / 0.1	36 / 0.4	37	40	38 / 0.25
	70–190	36 / 0.8	34 / 0.8	35	35	35 / 0.8
SPAS-1	280–380	91 / 0.4	51 / 0.5	54	55	63 / 0.45
	420–530	108 / 0.3	61 / 0.1	50	45	66 / 0.2
	80–190	52 / 0.7	28 / 0.8	26	27	33 / 0.75
SPAS-2	280–380	98 / 0.2	78 / 0.7	80	86	85 / 0.45
	420–510	107 / 0.2	26 / 0.3	52	12	49 / 0.25
	80–200	49 / 0.8	26 / 0.9	28	28	33 / 0.85
SPAS-3	280–340	41 / 0.9	93 / 1.6	98	102	83 / 1.25
	430–520	85 / 0.1	41 / 0.1	37	37	50 / 0.1
	60–200	31 / 0.5	38 / 0.7	40	41	37 / 0.6
SPAS-4	300–390	85 / 0.8	90 / 0.5	20	16	53 / 0.65
	60–170	42 / 0.5	18 / 0.4	21	20	25 / 0.45
SPAS-5	270–390	112 / 0.4	59 / 0.4	65	65	76 / 0.4
	60–160	28 / 0.2	22 / 0.5	23	24	24 / 0.35
SPAS-6	280–380	66 / 0.2	78 / 0.6	64	85	73 / 0.4

^{a)} Values of n calculated by Freeman-Carroll methods [5].

^{b)} Values of n calculated by Friedman methods [6].

components in the composite or its structural properties. The interaction between the silica and the polymer in the composite is of particular interest, and the calculation of kinetic parameters such as energy and thermal decomposition reaction sequence can help to consider the relationship between the silica backbone and the polymer network in the composite structure.

Kinetic analysis

The apparent activation energy (E_a), and reaction order (n) of the thermal decompositions were calculated from TG curves according to methods of Freeman-Carroll [5], Friedman [6] and Chang [7] using modified Arrhenius equation [5], which is solved graphically; where α is the mass loss over time t , $d\alpha/dt$ is the decomposition rate, Z is frequency factor, n is the decomposition reaction ratio, E is the energy of the activation, R is the gas constant ($8.3136 \text{ J mol}^{-1} \text{ K}^{-1}$) and T is the absolute temperature. Results of calculation of the kinetic parameters (E_a and n) are listed in Table 4.

Generally, direct comparison of the kinetic parameters obtained by different computational methods is very problematic because it is unclear whether the observed differences in the values originate from differences in the experimental conditions or from the differences in the computational methods [20].

CONCLUSIONS

Porous SPA/silica nanocomposites with different silica content were synthesized by sol-gel process. Post-synthetic treatment of transparent gels leads to minor changes in the nanocomposites structure but increases the specific surface area and sorption volume. The TG analysis suggests that the changes in the specific surface area shifts the thermal degradation to the lower temperature. However, no relationship between the energetic activation of thermal degradation and the value of the specific surface area was observed.

REFERENCES

- [1] Brinker C., Scherer G.W.: "Sol-Gel Science: The Physics and Chemistry of Sol-Gel Processing", Academic Press, New York 1990, p. 912.
<https://doi.org/10.1016/C2009-0-22386-5>
- [2] Ahmad Z., Mark J.E.: *Chemistry of Materials* **2001**, 13, 3320.
<https://doi.org/10.1021/cm010175n>
- [3] Morikawa A., Iyoku Y. *et al.*: *Polymer Journal* **1992**, 24, 107.
<http://dx.doi.org/10.1295/polymj.24.107>
- [4] Nakanishi K., Takahashi R. *et al.*: *Journal of Non-Crystalline Solids* **1992**, 147–148, 291.
[https://doi.org/10.1016/S0022-3093\(05\)80632-5](https://doi.org/10.1016/S0022-3093(05)80632-5)
- [5] Freeman E.S., Carroll B.: *Journal of Physical Chemistry* **1958**, 62, 394.
<https://doi.org/10.1021/j150562a003>
- [6] Friedman H.L.: *Journal of Polymer Science Part B: Polymer Letters* **1969**, 7, 41.
<https://doi.org/10.1002/pol.1969.110070109>
- [7] Chang W.L.: *Journal of Applied Polymer Science* **1994**, 53, 1759.
<https://doi.org/10.1002/app.1994.070531306>
- [8] Rouquerol F., Rouquerol J., Sing K.: "Adsorption by Powders and Porous Solids. Principles, Methodology and Application", Academic Press, San Diego, 1999, p. 467.
<https://doi.org/10.1016/B978-0-12-598920-6.X5000-3>
- [9] Barrett E.P., Joyner L.G., Halenda P.P.: *Journal of the American Chemical Society* **1951**, 73, 373.
<https://doi.org/10.1021/ja01145a126>
- [10] Avnir D., Jaroniec M.: *Langmuir*. **1989** 5, 1431.
<https://doi.org/10.1021/la00090a032>
- [11] Lee C.-K., Tsay C.-S.: *Journal of Physical Chemistry B* **1998**, 102, 4123.
<https://doi.org/10.1021/jp9803485>
- [12] Schull C.G.: *Journal of the American Chemical Society* **1948**, 70, 1405.
<https://doi.org/10.1021/ja01184a034>
- [13] Gavrilko T., Gnatyuk I., *et al.*: *Vibrational Spectroscopy* **2000**, 23, 199.
[https://doi.org/10.1016/S0924-2031\(00\)00060-6](https://doi.org/10.1016/S0924-2031(00)00060-6)
- [14] Mondragyn M.A., Castaco V.M., *et al.*: *Vibrational Spectroscopy* **1995**, 9, 293.
[https://doi.org/10.1016/0924-2031\(95\)00002-C](https://doi.org/10.1016/0924-2031(95)00002-C)
- [15] Cardenas G., Mucoz C., Carbacho H.: *European Polymer Journal* **2000**, 36, 1091.
[https://doi.org/10.1016/S0014-3057\(99\)00187-1](https://doi.org/10.1016/S0014-3057(99)00187-1)
- [16] Maurer J.J., Eustace D.J., Ratcliffe C.T.: *Macromolecules* **1987**, 20, 196.
<https://doi.org/10.1021/ma00167a035>
- [17] Kashiwagi T., Morgan A.B., *et al.*: *Journal of Applied Polymer Science* **2003**, 89, 2072.
<https://doi.org/10.1002/app.12307>
- [18] Gyulai G., Greenhow E.J.: *Journal of Thermal Analysis and Calorimetry* **1974**, 6, 279.
<https://doi.org/10.1007/BF01950059>
- [19] Broido A.: *Journal of Polymer Science Part A-2: Polymer Physics* **1969**, 7, 1761.
<https://doi.org/10.1002/pol.1969.160071012>
- [20] Maciejewski M.: *Thermochimica Acta* **2000**, 355, 145.
[https://doi.org/10.1016/S0040-6031\(00\)00444-5](https://doi.org/10.1016/S0040-6031(00)00444-5)

Received 25 X 2022.